



Analytical modeling of the interaction between skyrmions and extended defectsLeonardo González-Gómez, Josep Castell-Queralt, Nuria Del-Valle, Alvaro Sanchez, and Carles Navau *
Departament de Física, Universitat Autònoma de Barcelona, 08193 Bellaterra, Barcelona, Catalonia, Spain (Received 15 May 2019; revised manuscript received 12 July 2019; published 26 August 2019)

The performance of skyrmion-based spintronic devices can be greatly affected by the presence of defects in the materials. Here we develop an analytic model for describing the interaction between skyrmions and defects in ultrathin films focusing on the case of extended defects. The dynamics of skyrmions under the driving of in-plane polarized current is studied, considering several types of torques. The system is modeled with Thiele's equation in the complex plane and described with a reduced number of parameters. We start by considering a Gaussian-like interaction with point defects and extend the treatment to segment, line, and grid defects. Conditions for dynamic regimes of pinning, guiding, accelerating, or arranging skyrmions by defects are established and discussed. In particular, expressions for the threshold driven current density to pin or depin skyrmions in such defects, the position of the critical points, as well as the guiding conditions along long defects are found, analytically in some cases. This enables a deeper understanding of the parameter dependence of the skyrmion dynamics under the influence of defects. Micromagnetic simulations show qualitative agreement with the analytical treatment.

DOI: [10.1103/PhysRevB.100.054440](https://doi.org/10.1103/PhysRevB.100.054440)**I. INTRODUCTION**

Defects are ubiquitous in materials. From atomic to macroscopic scale, they can drastically affect some of the main properties of materials. For example, the introduction of small amounts of foreign atoms can drastically change the conductivity of semiconductors [1]. In superconducting materials, the introduction of controlled defects is a long-standing strategy to increase their critical-current density [2,3]. The optical, electronic, mechanical, and magnetic properties of graphene and other two-dimensional materials are also being tuned by defect engineering [4–6]. In general, the ultimate control of the physical properties of materials requires knowledge of the effect of defects over them.

In the case of magnetic materials, the defects not only change the magnetization properties [7], but they can also have a strong influence in the nucleation and motion of the magnetic structures that can be generated and moved in them, such as domain walls [8], vortices [9,10], or, particularly interesting for the present work, skyrmions [11–18].

Indeed, there is a large interest in the study of the dynamics of skyrmions, magnetic structures that can be stabilized in ferromagnetic thin films with the aid of interfacial Dzyaloshinskii-Moriya (DM) interaction with a nonmagnetic heavy-metal substrate with strong spin-orbit coupling [14,15,19,20]. The relevance of these works relies on the fact that skyrmions are small in size, can be driven by low-density spin-polarized currents, and can be stabilized at room temperature [15,17,21–25]. They have the potential for becoming information carriers in next-generation ultradense magnetic memories, logic devices, or computational systems [26–30].

Defects in the material where skyrmions are nucleated affect their dynamics. The presence of a threshold current density for moving skyrmions has been attributed to the

presence of randomly distributed defects or grains [31–34]. A global phenomenological friction force was considered to account for these randomly distributed impurities [35–37]. Also, it has been shown that local variations of magnetic properties [38–44] have relevant influence over the skyrmions. In particular, Müller and Rosch [38] considered a vacancy in the magnetization distribution and evaluated numerically the energy coming from the resulting system. The fitting of the energy allowed one to find an effective numerical pinning potential and to study the dynamics of skyrmions in the presence of this potential. Choi *et al.* [43], in a more atomistic treatment, used density functional theory to study the influence of atomic modifications over skyrmions. Their conclusions were based on the electronic density of states without focusing on the particular dynamics of the skyrmion. Hanneken *et al.* [39] used scanning tunneling microscopy to find profiles of the pinning potential created by defects of different origins (local variation of anisotropy, exchange, or DM interactions). In [44], analytic expressions for the forces acting over a skyrmion considering also different local variations of interaction parameters were derived without exploring the dynamics produced by these forces.

Other types of phenomenologically introduced potentials have also been used to describe particular cases. For example, periodic potentials have been introduced to simulate periodic substrates [45,46], and linear forces (harmonic potentials) to describe pinning sites [41,47], or several types of potentials to describe the effect of borders [23,48–52]. In most of these works, the skyrmion dynamics is studied through Thiele's equation [53]. In this approximation, the skyrmion is treated as a rigid object, without internal degrees of freedom, and following a non-Newtonian dynamical equation in which the external potentials enter as extra terms in the equation. This rigid model, valid as long as the skyrmion is not substantially deformed during the movement, helps to set the relevant parameters of the dynamics, to establish the relevant orders

*Corresponding author: carles.navau@uab.cat

of magnitude of the physical magnitudes involved, as well as to find the dependence of these magnitudes upon the relevant parameters.

In spite of all these efforts, a general and systematic analytic treatment of the skyrmion-defect interaction and the resulting dynamics is still lacking, especially when considering extended defects, where it has been recently numerically found that this kind of defect can accelerate and guide skyrmions along predefined defect paths [54]. Here, we fill this gap by developing an analytic model of the skyrmion-defect interaction and, from this interaction and using Thiele's equation, describe the dynamics of the skyrmions in the presence of defects. The starting point is the interaction of a skyrmion with a point defect modeled as a Gaussian-like potential (a good approximation of what was found in [38,44] or in [55,56] for vortices). This potential is extended here to account for elongated defects. The analytic treatment is verified by numerical simulations.

The rest of the paper is structured as follows. In Sec. II we present an alternative Thiele's equation in complex form. In Sec. III, we present the model for skyrmion-point defect interaction. In Sec. IV the treatment is extended to consider linear defects, including finite, infinite, L-shaped, and cross-shaped cases. The case of a grid of defects is treated in Sec. V. Some final remarks are presented in Sec. VI.

II. THE RIGID (THIELE'S) MODEL FOR THE DYNAMICS OF SKYRMIONS

A. Torques over the magnetic structure

Within the micromagnetic model used in this work, the magnetization structure in a ferromagnet is considered as a continuous magnetization function $\mathbf{M}(\mathbf{r})$ of the position \mathbf{r} inside the ferromagnet. It is assumed that the modulus of \mathbf{M} is constant and uniform, $|\mathbf{M}| = M_s$ (the saturation magnetization), and that the variation of this function with time results in the dynamics of the magnetization structures that can be formed in the material. These dynamics can be evaluated through the Landau-Lifshitz-Gilbert equation, which reads

$$\frac{d\mathbf{M}}{dt} = -\gamma\mathbf{M} \times \mathbf{H}_{\text{eff}} + \frac{\alpha}{M_s}\mathbf{M} \times \frac{d\mathbf{M}}{dt} + \mathbf{T}. \quad (1)$$

\mathbf{H}_{eff} is the effective field and contains the different interactions that describe the system (in our case, we consider exchange, uniaxial anisotropy, and DM), $\gamma = 2.21 \times 10^5 \text{ m A}^{-1} \text{ s}^{-1}$ is the gyromagnetic constant, α is a positive dimensionless constant (Gilbert constant) accounting for the damping of the precession of the magnetization around the axis defined by the direction of the effective field, and \mathbf{T} represents extra torques that could affect the magnetization distribution.

In this work we focus on a thin planar ferromagnetic layer of thickness d deposited on top of a heavy-metal substrate with strong spin-orbit coupling (see Fig. 1). We consider that d is small enough so that all magnitudes are assumed uniform across the thickness. The ferromagnetic layer is located on the xy plane.

When applying a current perpendicular to the ferromagnetic plane and spin polarized in the direction \mathbf{m}_p , two torques appear, $\mathbf{T}_1 \propto \mathbf{M} \times (\mathbf{m}_p \times \mathbf{M})$ and $\mathbf{T}_2 \propto -\mathbf{M} \times \mathbf{m}_p$. These torques can trigger the nucleation of skyrmions [40,57]

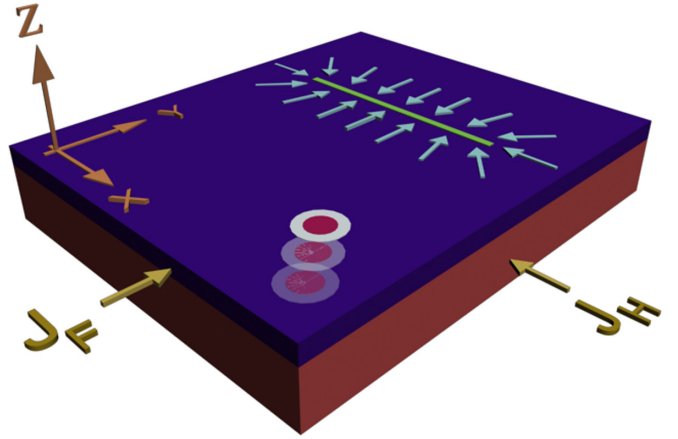


FIG. 1. Sketch of the considered system. \mathbf{J}_F and \mathbf{J}_H represent the current densities flowing in the ferromagnet (blue region) and the heavy metal (red region), respectively. The skyrmion (red-white circular structure) moves towards the defect (green line), whose attractive force is represented by a vector field (light-blue arrows).

and skyrmionic spin-torque-driven nano-oscillators [57,58]. However, the driving of skyrmions is usually done through in-plane currents [59]. Here we will focus on this latter case.

If an in-plane current-density $\mathbf{J}_F = J_F \hat{\phi}$ ($\hat{\phi}$ has only \hat{x} and \hat{y} components) flows through the ferromagnet, in the adiabatic approximation the spins of this current align in the direction of the magnetization, resulting in a reaction torque over the magnetization [60]

$$\mathbf{T}_3 = -\frac{\mu_B P J_F}{e M_s^3} \mathbf{M} \times [\mathbf{M} \times (\hat{\phi} \cdot \nabla) \mathbf{M}] = \frac{\mu_B P J_F}{e M_s} (\hat{\phi} \cdot \nabla) \mathbf{M}, \quad (2)$$

where μ_B is the Bohr magneton, e the charge of the electron ($e > 0$), and P is the spin-polarization factor of the current. When there is some spatial mistracking of the spins of the conduction electrons and the local magnetization (nonadiabatic approximation) an extra torque term appears, given by [61,62]

$$\mathbf{T}_4 = -\beta \frac{\mu_B P J_F}{e M_s^2} \mathbf{M} \times (\hat{\phi} \cdot \nabla) \mathbf{M}, \quad (3)$$

where β is a dimensionless constant accounting for the nonadiabaticity of the spin alignment with the local magnetization.

If another in-plane current flows through the heavy metal with current density $\mathbf{J}_H = J_H \hat{\eta}$ ($\hat{\eta}$ has also only \hat{x} and \hat{y} components), it generates, due to the spin-Hall effect (SHE) in the heavy metal, an accumulation of spin-polarized electrons on the interface which are polarized in the $\hat{\sigma} = \hat{z} \times \hat{\eta}$ direction. These spin-polarized electrons diffuse into the ferromagnet generating a dampinglike torque given by [63]

$$\mathbf{T}_5 = -\frac{\mu_B \theta_H J_H}{e M_s^2 d} \mathbf{M} \times [\mathbf{M} \times \hat{\sigma}], \quad (4)$$

where θ_H is the spin Hall angle factor. It represents the ratio between the electronic current density through the heavy metal and the spin-polarized current density diffusing through the ferromagnet. There also appears a fieldlike torque given by [64]

$$\mathbf{T}_6 = -v \frac{\mu_B \theta_H J_H}{e M_s d} \mathbf{M} \times \hat{\sigma}, \quad (5)$$

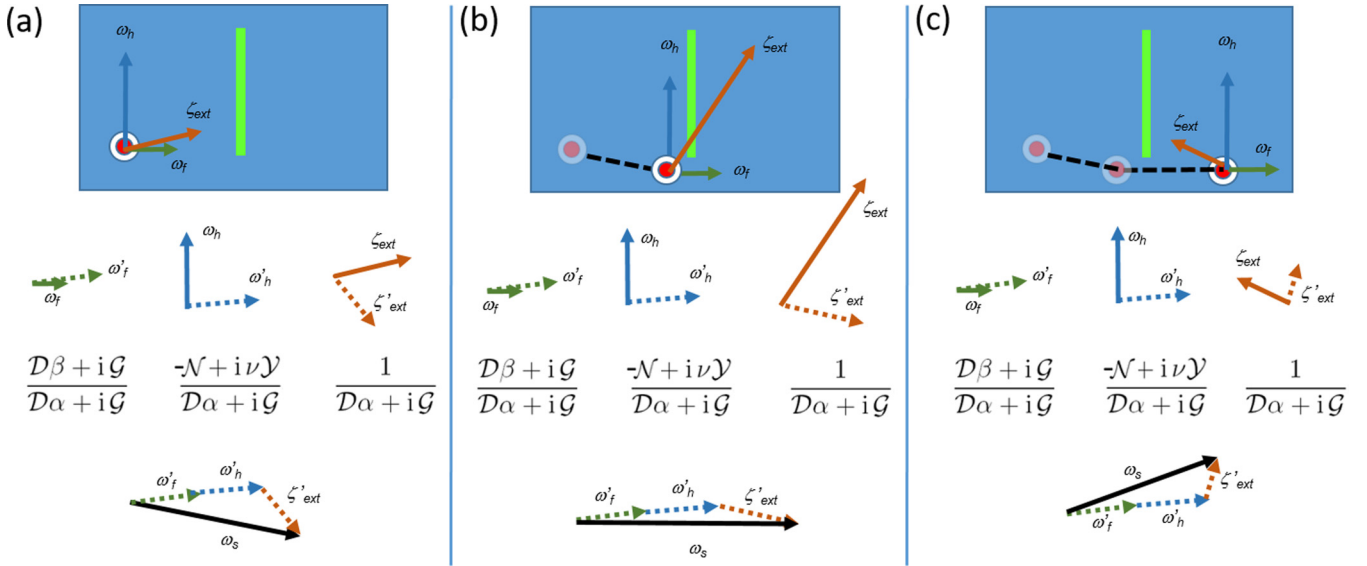


FIG. 2. Sketch for the geometrical interpretation of the complex version of Thiele's equation. The skyrmion is represented by the red-white circle, and a linear defect by the green vertical line. Different vectors correspond to the different complex velocities or external forces, using the same notation as in the text. The rotated and rescaled vectors [according to the indicated complex constants; see Eq. (14)] are represented as dotted vectors and primed (') magnitudes. The velocity of the skyrmion at the present point, ω_s , is the sum of the dotted vectors [Eq. (15)]. In (b) the situation is repeated for a new position of the skyrmion. For uniform current densities only the external force ζ_{ext} changes. The new velocity is found in the same way when the skyrmion is at the position indicated in (c).

where ν is a dimensionless parameter indicating the strength of \mathbf{T}_6 with respect to \mathbf{T}_5 .

B. Thiele's equation: Definitions and normalization

Thiele's equation can describe the rigid (without internal degrees of freedom) movement of a magnetic structure. Within this approximation the dynamics of a skyrmion is characterized by the movement of its center-of-mass position \mathbf{r}_s (and velocity \mathbf{V}_s) on the xy plane. That is, under the assumption of $\mathbf{M}(\mathbf{r}) = \mathbf{M}_0[\mathbf{r} - \mathbf{r}_s(t)]$ where \mathbf{M}_0 represents the magnetization distribution centered at $\mathbf{r} = 0$, and following the derivations in [53], Eq. (1) becomes

$$(\mathbb{G} - M_s \alpha \mathbb{D}) \mathbf{V}_s + \gamma M_s^2 \mathbf{F}_{\text{ext}} - (\mathbb{G} - M_s \beta \mathbb{D}) \mathbf{V}_F + M_s (\mathbb{N} + \nu M_s \mathbb{Y}) \mathbf{V}_H = 0, \quad (6)$$

where the elements of the matrices \mathbb{G} , \mathbb{D} , \mathbb{N} , and \mathbb{Y} , and the definitions of the vectors \mathbf{V}_F , \mathbf{V}_H , and \mathbf{F}_{ext} are given by

$$\mathbb{G}_{uv} = \int_V \mathbf{M}_0 \cdot \left(\frac{\partial \mathbf{M}_0}{\partial u} \times \frac{\partial \mathbf{M}_0}{\partial v} \right) dV, \quad (7)$$

$$\mathbb{D}_{uv} = \int_V \left(\frac{\partial \mathbf{M}_0}{\partial u} \cdot \frac{\partial \mathbf{M}_0}{\partial v} \right) dV, \quad (8)$$

$$\mathbb{N}_{uv} = \frac{1}{d} \int_V \left(\frac{\partial \mathbf{M}_0}{\partial u} \times \mathbf{M}_0 \right)_v dV, \quad (9)$$

$$\mathbb{Y}_{uv} = \frac{1}{d} \int_V \frac{\partial M_{0,v}}{\partial u} dV, \quad (10)$$

$$(\mathbf{F}_{\text{ext}})_u = \int_V \mathbf{H}_{\text{ext}} \cdot \frac{\partial \mathbf{M}_0}{\partial u} dV, \quad (11)$$

$$\mathbf{V}_F = -\frac{\mu_B P}{e M_s} \mathbf{J}_F, \quad (12)$$

$$\mathbf{V}_H = -\frac{\mu_B \theta_H}{e M_s} (\hat{\mathbf{z}} \times \mathbf{J}_H). \quad (13)$$

In the above equations, u and v are either x or y . V is the volume where the magnetization changes. \mathbf{H}_{ext} is the effective field due to external interactions. The first term in Eq. (6) contains the Magnus and the dissipation terms that depend on the velocity of the skyrmion. The second term is due to external forces acting over the skyrmion (such as pinning, borders, gradient of fields or temperature, substrate, etc.). The third term comes from the spin-transfer torque of the current flowing in the ferromagnet, and the last term arises from the SHE-induced spin-polarized currents in the heavy metal. Note that \mathbf{V}_s , \mathbf{V}_F , and \mathbf{V}_H have units of velocity.

In the rest of the paper we consider a radially symmetric skyrmion on a ferromagnetic background pointing to $-\hat{\mathbf{z}}$. In this case $\mathbb{G}_{xy} = -\mathbb{G}_{yx} \equiv G$, $\mathbb{D}_{xx} = \mathbb{D}_{yy} \equiv D$, $\mathbb{N}_{xy} = -\mathbb{N}_{yx} \equiv -N$, and $\mathbb{Y}_{xx} = \mathbb{Y}_{yy} = Y$. All other elements of the matrices are zero. With the present definitions and background, $G > 0$, $D > 0$, $N > 0$, and $Y > 0$.

It is convenient to normalize Eq. (6) and use nondimensional variables. We use for normalization a typical length involved in the system L (could be the radius of the skyrmion, the exchange length, etc.), the typical time $t_0 = (\gamma M_s)^{-1}$, and define the dimensionless variables $\mathcal{G} = G/(M_s^3 d)$, $\mathcal{D} = D/(M_s^2 d)$, $\mathcal{N} = N/(M_s^2 L)$, $\mathcal{Y} = Y/(M_s^3 L)$, $\mathbf{v}_{s,f,h} = \mathbf{V}_{s,F,H}/(\gamma M_s L)$, and $\mathbf{f}_{\text{ext}} = \mathbf{F}_{\text{ext}}/(M_s^2 d L)$. Alternatively, in the present two-dimensional case, Eq. (6) can be rewritten in terms of complex variables [65–67]. Defining $\omega_{(s,f,h)} \equiv v_{(s,f,h),x} + i v_{(s,f,h),y}$, $\zeta_{\text{ext}} = f_{\text{ext},x} + i f_{\text{ext},y}$ for the velocities and external forces, respectively, Eq. (6) is converted to

$$\omega_s = \frac{1}{\mathcal{D}\alpha + i\mathcal{G}} \zeta_{\text{ext}} + \frac{\mathcal{D}\beta + i\mathcal{G}}{\mathcal{D}\alpha + i\mathcal{G}} \omega_f + \frac{-\mathcal{N} + i\nu\mathcal{Y}}{\mathcal{D}\alpha + i\mathcal{G}} \omega_h. \quad (14)$$

The geometrical interpretation of Thiele's equation is sketched in Fig. 2. ω_s , ζ_{ext} , ω_f , and ω_h can be represented as vector fields in the complex plane. For each position of the skyrmion (a point in the complex plane), ω_s , ω_h , and the external force ζ_{ext} are rescaled and rotated according to the complex constant that accompanies them in Eq. (14). The rescaling is equal to the modulus of the constant and the angle of rotation is equal to its argument. Once rotated and rescaled, the complex velocity of the skyrmion at each point can be just obtained as the sum of three complex numbers

$$\omega_s = \zeta'_{\text{ext}} + \omega'_f + \omega'_h, \quad (15)$$

with $\zeta'_{\text{ext}} = \zeta_{\text{ext}}/(\mathcal{D}\alpha + i\mathcal{G})$, $\omega'_h = \omega_h(-\mathcal{N} + iv\mathcal{Y})/(\mathcal{D}\alpha + i\mathcal{G})$, and $\omega'_f = \omega_f(\mathcal{D}\beta + i\mathcal{G})/(\mathcal{D}\alpha + i\mathcal{G})$.

The previous expression indicates that whatever the origin and directions of the driving current densities, all the torques can be put together in a single term $\omega' = \omega'_f + \omega'_h$, which is unambiguously defined after knowing \mathbf{J}_F and \mathbf{J}_H and the constants \mathcal{G} , \mathcal{D} , \mathcal{N} , and \mathcal{Y} . Several combinations of ω_f and ω_h , or modification of polarization direction [68] can be considered in this way.

One of the key aspects when solving the previous equation is to find the critical points of the trajectory of skyrmions. They are defined as those points with $\omega_s = 0$.

In order to simplify our treatment, in the following sections we consider that currents flow uniformly. Without loss of generality, we also consider $\omega_f = 0$ ($J_F = 0$) and $v = 0$. Just a rescaling and rotation of the global vector field $\omega_f + \omega_h$ would be enough to consider $\omega_f \neq 0$ and/or $v \neq 0$. Note that in the present treatment we are also assuming that the defects are far from the edges of the ferromagnetic sample. Using exponential [48], harmonic [47], oscillating [23], or other forces, one could consider also the effect of the presence of edges just by adding an extra ζ function coming from them. We will also use $\omega_h = v_h e^{i\varphi_h}$, φ_h being the angle between the direction of the current density in the heavy metal and the x axis. Moreover, from now on, we use for the (complex, normalized) position the standard notation $z = x + iy$, since there is no confusion with the real-space z coordinate (which is always, by construction, zero in the present planar system).

III. SKYRMION-POINT DEFECT INTERACTION

Consider a point defect localized at the origin of coordinates. We choose the current density to flow along the x axis ($\varphi_h = 0$, thus ω_h is a real number $\omega_h = v_h$). According to [38,44,69], different types of point defects (created by a diversity of local mechanisms) generate different forces over the skyrmion. When the defect is considered as a local variation of the DM interaction, the force can be well approximated by a radially symmetric force, that linearly increases close to the pinning center and decays when far from it. An adequate potential for describing this force is a Gaussian-like function $U(\rho) = -U_0 e^{-\rho^2/\lambda_0^2}$, where λ_0 (>0) is a parameter that indicates the radial scope of the defect and U_0 its intensity. ρ is the radial distance from the origin. (Other types of defects can also be approximated by similar functions, as discussed at the end of this section; for simplicity we choose here this Gaussian-like potential.) Here we consider attractive defects, so that $U_0 > 0$. The force created by this kind of potential is $\mathbf{F}_{\text{ext}} = \mathbf{F}_{\text{pnt}} = -(2U_0/\lambda_0^2)\rho e^{-\rho^2/\lambda_0^2}\hat{\rho}$. In the complex

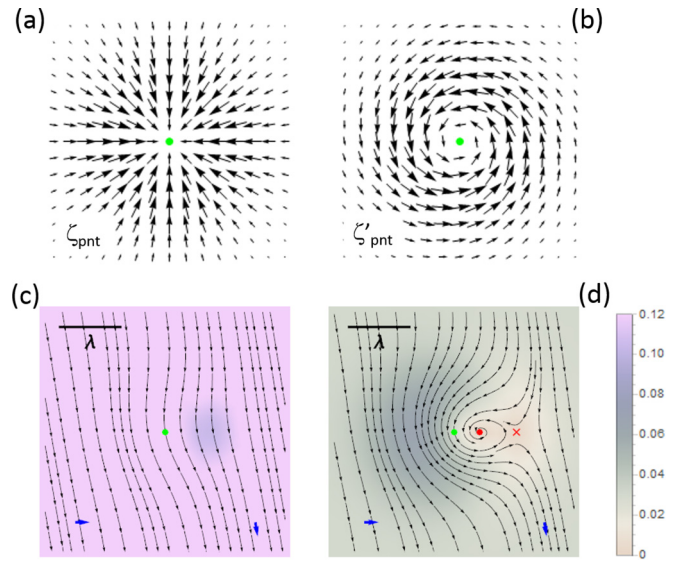


FIG. 3. (a) The vector field corresponding to ζ_{pnt} attractive Gaussian-like forces [Eq. (16)]; (b) the vector field corresponding to ζ'_{pnt} ; (c),(d) phase portraits of Thiele's equation considering driving velocities v_h below (c) and above (d) the threshold value [Eq. (18)]. The background color [in (c) and (d)] indicates the speed of the skyrmions. The green dot corresponds to the position of the defect. The red dot (cross) indicates the position of the attractor (saddle) point. Blue arrows indicate the direction of the driving current density ω_h (left) and the direction of the velocity of skyrmion in the absence of defects ω'_h (right). In this particular example $\mathcal{G} = 3\pi$, $\mathcal{D} = 5\pi$, $\mathcal{N} = 2\pi$, $\lambda = 1$, $\zeta_0 = 1$, $\alpha = 0.1$, and $v_h = v_{\text{th,pnt}}/2$ and $2v_{\text{th,pnt}}$. The black line indicates the length scale.

normalized form, one finds

$$\zeta_{\text{pnt}}(z) = -\zeta_0 z e^{-|z|^2/\lambda^2}, \quad (16)$$

where $\zeta_0 = 2U_0 L/\lambda_0^2$ and $\lambda = \lambda_0/L$ are dimensionless parameters.

Inserting this force into Eq. (14) one sees that there are, at most, two critical points located on the axis of application of current, at positions $x = s\lambda_0$ where the two s values are the solutions of the real equation

$$s e^{-s^2} = \frac{\mathcal{N} v_h}{\lambda \zeta_0}. \quad (17)$$

When they exist, the two solutions can be classified into a spiral attractor point z_\bullet (the solution closer to the origin), and a saddle point z_\times . The condition of existence of these solutions sets a threshold value for the velocity v_h , below (above) which there can (cannot) exist critical points. This threshold value is found to be

$$v_{\text{th,pnt}} = \frac{\lambda \zeta_0}{\sqrt{2e} \mathcal{N}}. \quad (18)$$

Note that $v_{\text{th,pnt}}$ does not depend on α . We show in Fig. 3(a) the vector field corresponding to the Gaussian force $\zeta_{\text{pnt}}(z)$ and in Fig. 3(b) the corresponding rescaled and rotated $\zeta'_{\text{pnt}}(z)$. In Figs. 3(c) and 3(d) we show the phase portraits of Thiele's equation [Eq. (14)] when the driving current density is below and above the threshold value, respectively. The presence of a spiral trapping point z_\bullet does not mean that the skyrmion will always be trapped, but that it *can* be trapped if it passes

close enough to the attractive point (as described in [38] using numerical simulations).

The harmonic pinning potential can be obtained as a limiting case of the present Gaussian-like potential when the skyrmion is close (as compared with λ_0) to the pinning center, $U(\rho) \simeq U_0[1 - (\rho/\lambda_0)^2]$ for $\rho \ll \lambda_0$. In this case one recovers the known damped spiral trajectories, in the present case around the critical point $z_* = v_h \mathcal{N} / \zeta_0$ [41,47,48,70].

A natural extension of the present Gaussian-like potential could be applied when the defect produces an attractive force at short distances but repulsive far from it. This is the case, for example, of defects produced by local variation of anisotropy [44] and also could be a good approximation for the potential created by holes or other local defects [38,71]. In this case, a good approximation (useful for the analytical treatment) of the potential could be obtained by adding an extra b term acting at larger distances: $U = -U_0(1 - b \frac{\rho^2}{\lambda_0^2})e^{-\rho^2/\lambda_0^2}$, which results in the normalized complex form

$$\zeta(z) = -\zeta_0 z \left(1 - b \left[\frac{|z|^2}{\lambda^2} - 1 \right] \right) e^{-|z|^2/\lambda^2}. \quad (19)$$

In this case, several scenarios can appear with respect to the parameters. One finds that for small current densities, there are four critical points (two saddles, one repulsive, and one attractor), at intermediate velocities there are two critical points (one attractor and one saddle), and for large velocities there are no critical points.

IV. LINE DEFECTS

When a defect is large as compared with the dimensions of the skyrmion, it can no longer be considered as a pointlike

defect. Actually, a common defect is an elongated one produced by dislocations or grain boundaries in a thin film. Little work has been devoted to the description of line defects, especially finite ones. In this section we extend the analytic analysis to consider an extended finite line defect of (normalized) length a . The force created by line defects can be obtained by considering point defects very close one to each other. In this case the relevant magnitude is the *density* of force as the force of one defect divided by the distance between two consecutive defects, Δ (normalized). Δ can be associated to the interatomic distance. Studying systems at scales $a \gg \Delta$ enables the use of the continuous limit. The force is then evaluated as the integral of the contribution along all the continuous extension of the defects

$$\zeta_{\text{sgm}}(z) = \int_l \frac{1}{\Delta} \zeta_{\text{pnt}}(z - z_0) dz_0, \quad (20)$$

where l indicates the segment over which the defects are extended. Now, the angle at which the current is applied with respect to the defect line will influence the trajectories of the skyrmions.

Consider a segment defect located at $x \in [-a/2, a/2]$ and that the current is applied at an angle φ_h with respect to this x axis: $\omega_h = v_h e^{i\varphi_h}$. The force can be analytically evaluated after Eq. (20) using Eq. (16) for the point force. The result is

$$\zeta_{\text{sgm}}(z) = \frac{\zeta_0 \lambda^2}{2\Delta} \left[L \left(\frac{\text{Re}(z) - a/2}{\lambda}, \frac{\text{Im}(z)}{\lambda} \right) - L \left(\frac{\text{Re}(z) + a/2}{\lambda}, \frac{\text{Im}(z)}{\lambda} \right) \right], \quad (21)$$

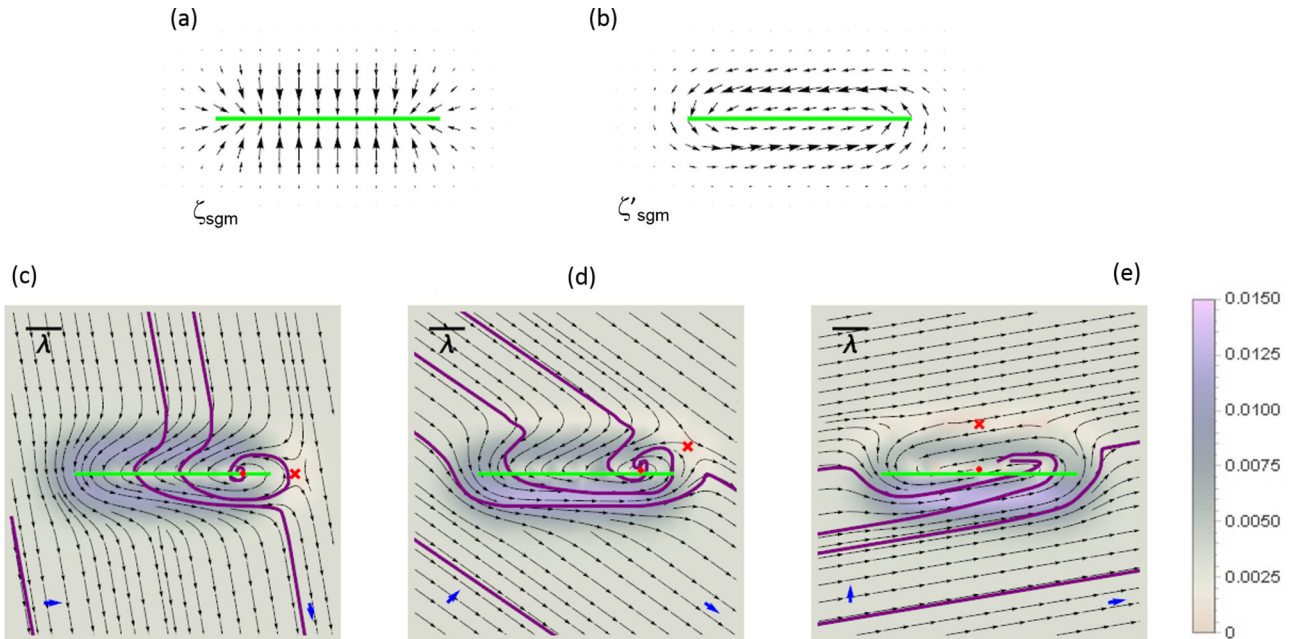


FIG. 4. (a) Vector field corresponding to the force ζ_{sgm} produced by a segment [Eq. (21)]. (b) The corresponding ζ'_{sgm} vector field. (c)–(e) Phase portrait of Thiele's equation for the finite segment for different values of the driving angle (c) $\varphi = 0$, (d) $\varphi = \pi/4$, and (e) $\varphi = \pi/2$. The solid purple lines correspond to trajectories of the center of a skyrmion calculated solving the Landau-Lifshitz-Gilbert equation for several initial positions. The meaning of symbols, bars, and arrows is the same as in Fig. 3. For these particular plots $\mathcal{G} = 3\pi$, $\mathcal{D} = 5\pi$, $\mathcal{N} = 2\pi$, $\zeta_0/\Delta = 0.13$, $\alpha = 0.1$, and $v_h = 0.0049$.

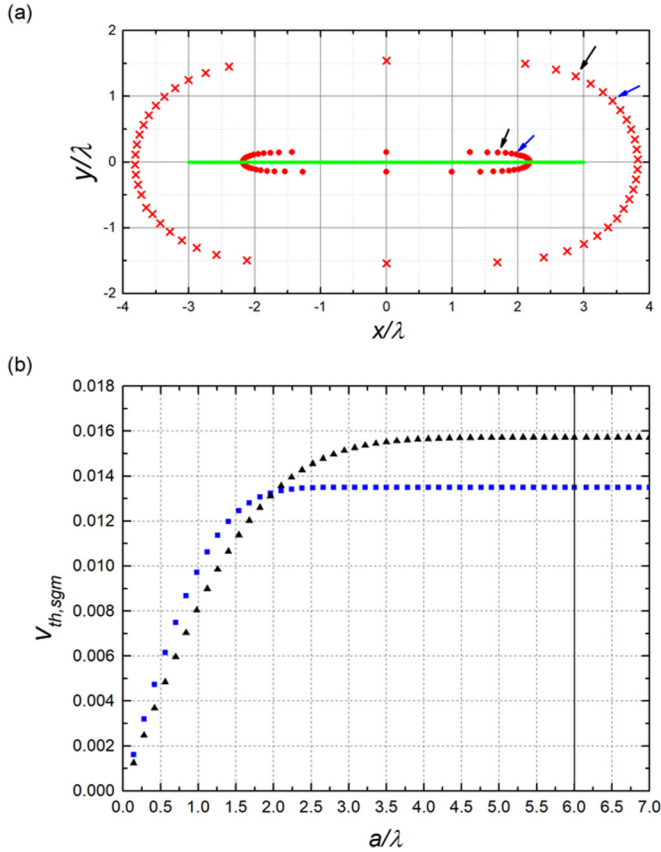


FIG. 5. (a) Position of the attractor points (red dots) and the saddle points (red crosses) for different angles of the driving current density. The defect is indicated by a green horizontal line; arrows indicate the critical points at the angles used in (b). (b) Threshold velocity as a function of the size of the defect, evaluated after Eq. (22), for two angles $\varphi_h = \pi/4$ (blue square) and $\varphi_h = 3\pi/8$ (black triangle). The vertical line indicates the size of the defect shown in (a). The parameters used in this case are $\mathcal{G} = 3\pi$, $\mathcal{D} = 5\pi$, $\mathcal{N} = 2\pi$, $\zeta_0/\Delta = 0.13$, $\alpha = 0.1$, and $v_h = 0.0049$.

where the function $L(u, v) = v^{-2} [e^{u^2} - i\sqrt{\pi}v \operatorname{erf}(u)]$. The $\operatorname{erf}(\cdot)$ function is the error function. $\operatorname{Re}(\cdot)$ and $\operatorname{Im}(\cdot)$ indicate the real and the imaginary part, respectively. In this case $\operatorname{Re}(z) = x$ and $\operatorname{Im}(z) = y$. The above expression recovers the limit of a point defect [Eq. (16)] for small a and considering $a = \Delta$. The field vector expressed in Eq. (21) is shown in Fig. 4(a) together with the corresponding ζ'_{sgm} vector field [Fig. 4(b)] and the phase portraits of Eq. (15) for current flowing parallel to the segment [$\varphi_h = 0$; Fig. 4(c)].

It is observed that there can be, in general, an attractive and a saddle point, their positions depending on the angle of the current, as indicated with dots and crosses, respectively, in Figs. 4(c)–4(e). The threshold velocity for having critical points depends on the length of the defect a and the angle φ_h , and is proportional to the minimum value between the two maximums of the real and imaginary parts of ζ_{sgm} :

$$v_{\text{th,sgm}} = -\frac{1}{\mathcal{N}} \min \left\{ \max \left[\frac{\operatorname{Re}[\zeta_{\text{sgm}}(z)]}{\cos \varphi_h} \right], \max \left[\frac{\operatorname{Im}[\zeta_{\text{sgm}}(z)]}{\sin \varphi_h} \right] \right\}. \quad (22)$$

In Fig. 5(a) we show the numerically found position of the critical points as a function of φ_h for a given length of the defect and a given velocity below the threshold. We observe that both the attractor and the saddle points move around the defect as the angle of the driving current changes. In Fig. 5(b) we show the numerically evaluated threshold velocity, $v_{\text{th,sgm}}$, as a function of a , for two particular angles of driving current. For other angles, one can find the threshold velocity using Eq. (22).

To confirm the analytic results we have performed micromagnetic calculations solving the Landau-Lifshitz-Gilbert dynamical equation. We have used the same homemade code as in [54] considering magnetization saturation $M_s = 580 \text{ kA m}^{-1}$, exchange interaction constant $A = 15 \text{ pJ m}^{-1}$, DM interaction constant $D_M = 3 \text{ mJ m}^{-2}$, uniaxial effective anisotropy constant $K = 0.425 \text{ MJ m}^{-3}$, Gilbert damping constant $\alpha = 0.1$, driving current densities $J_H = 1.75 \times 10^{10} \text{ A m}^{-2}$, and $\theta_H = -0.33$. The thickness has been fixed to $d = 1 \text{ nm}$. The defect has been simulated considering a local variation of the DM constant by a factor of 1.5, which results in a ζ_0/Δ fitting value of 0.13. λ has been taken as the radius of the skyrmion far from the defect (22 nm according to the micromagnetic simulations), so that $\lambda_0 = 1$. We show in Figs. 4(c)–4(e), the calculated micromagnetic trajectories for the center of the skyrmion. We observe a good agreement with Thiele's equation predictions. The discrepancies are associated to the fact that the skyrmion is deformed during the interaction with the defect line. However, this deformation is not drastic and Figs. 4(c)–4(e) demonstrate that Thiele's equation would be valid in this range of parameters.

An especially relevant limiting case is obtained when $a \gg \lambda$, corresponding to a linear defect much larger than the typical radius of the skyrmion. These kinds of defects were numerically studied in [54] using micromagnetic codes. As found numerically, skyrmions can be guided along the defect or can cross it if the driven velocity is above a given threshold. Analytically, the force exerted by the defect is, after Eq. (21) in the limit $a \rightarrow \infty$,

$$\zeta_{\text{infx}}(z) = -i \frac{\zeta_0 \lambda \sqrt{\pi}}{\Delta} \operatorname{Im}(z) e^{-\operatorname{Im}(z)^2/\lambda^2}. \quad (23)$$

In this case, no critical points exist (except when $\varphi = \pm\pi/2$). However, it is possible that the component of the velocity perpendicular to the defect line cancels, whereas the parallel component does not. This results in a guiding regime along the defect if the driving velocity is below

$$v_{\text{th,infx}} = \frac{\sqrt{\pi} \zeta_0 \lambda^2}{\mathcal{N} \Delta \sqrt{2} e} \sin \varphi_h, \quad (24)$$

which corresponds to the saturation value in Fig. 5(b). Moreover, when the skyrmion is guided along the defect line, $\omega_s = v_h \mathcal{G} \cos \varphi_h / (\alpha \mathcal{D})$ (a real value). This result indicates that the guiding velocity (i) does not depend on the parameters of the potential ζ_0 or λ (note that the conditions for being guided do depend on ζ_0 and on λ); and (ii) is inversely proportional to α , indicating the possibility of a large acceleration along the defect if α is small [47]. This $1/\alpha$ dependence is confirmed in the micromagnetic simulations performed with the above parameters.

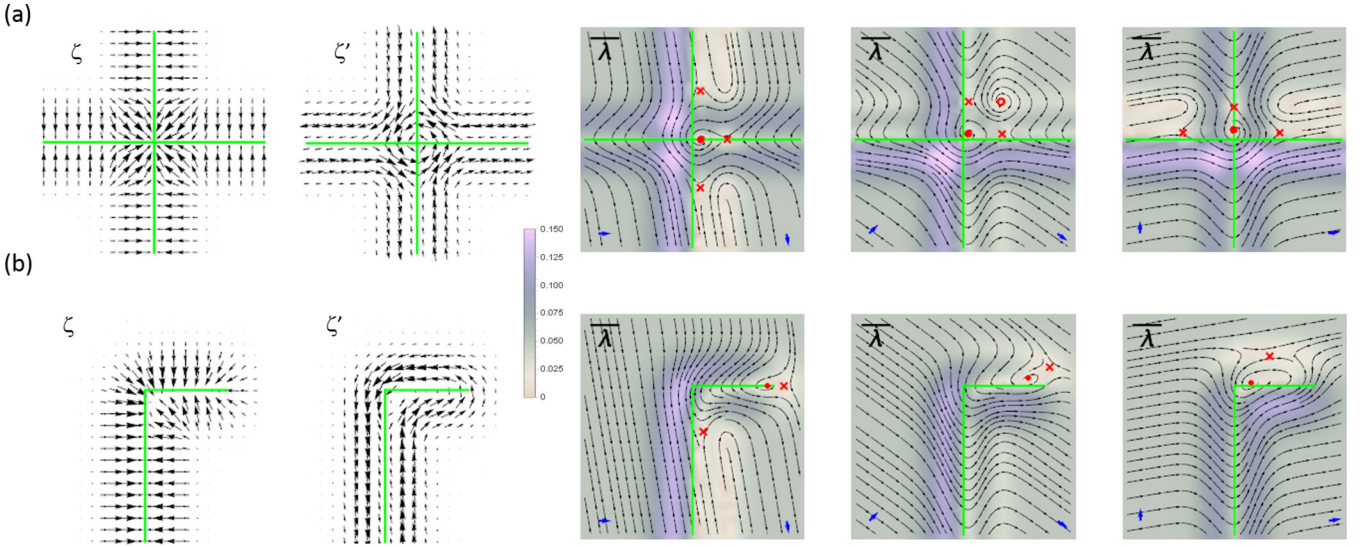


FIG. 6. Force vectors ζ_{sgm} and ζ'_{sgm} and phase portraits of Thiele's equation for an L-shaped [(a), upper row] and a cross-shaped [(b), lower row] defect. The phase portraits are shown for three different angles (from left to right $\varphi_n = 0, \pi/4$, and $\pi/2$). The meaning of symbols, bars, and arrows is the same as in Fig. 3; open red circle indicates repulsive critical point. For these particular plots $\mathcal{G} = 3\pi$, $\mathcal{D} = 5\pi$, $\mathcal{N} = 2\pi$, $\zeta_0/\Delta = 1.0$, $\alpha = 0.1$, and $v_h = 0.15$.

Another extension is to consider several defect shapes that could be obtained as a combination of finite segments. As examples, we show in Fig. 6 the velocity vector fields of the velocity for cross-shaped [Fig. 6(a)] and L-shaped [Fig. 6(b)] defects, as well as the corresponding phase portraits of Thiele's equation. As a general rule, when the defect ends or when there is a crossing or merging of defects in different directions, if the driven current density is below a given threshold, attractor points z_* , where the skyrmion can be trapped appear. In addition, we observe that in the cross-shaped case, close to the crossing point, there can appear repulsive critical points z_o , in addition to saddle points z_x . Also, when the defect is large enough in comparison with the typical range of the defect (λ) there can be guiding of skyrmions along defect lines.

V. GRID DEFECTS

The previous results of guiding skyrmions along defect lines and trapping them close to the crossing position with another perpendicular defect line open the possibility of having an artificial arrangement of skyrmions in a regular lattice. In this sense, consider a set of infinite-line defects arranged as a periodic rectangular grid, where the different lines are separated a distance δ_x in the x axis and δ_y in the y axis. Using Eq. (23) the total force at a given position z is described by

$$\zeta_{\text{grd}}(z) = -\zeta_0 \frac{\sqrt{\pi}\lambda}{\Delta} \left[\sum_{m=-\infty}^{\infty} (x - \delta_x m) e^{-(x - \delta_x m)^2 / \lambda^2} + i \sum_{n=-\infty}^{\infty} (y - \delta_y n) e^{-(y - \delta_y n)^2 / \lambda^2} \right]. \quad (25)$$

This expression can be expressed in terms of the elliptic theta prime functions $\vartheta'_n(\cdot)$ [72] as

$$\zeta_{\text{grd}}(z) = -\zeta_0 \frac{\pi^2 \lambda^4}{2\Delta} \left(\frac{1}{\delta_x^2} \vartheta'_3 \left(-\pi x / \delta_x | e^{-(\pi \lambda / \delta_x)^2} \right) + i \frac{1}{\delta_y^2} \vartheta'_3 \left(-\pi y / \delta_y | e^{-(\pi \lambda / \delta_y)^2} \right) \right). \quad (26)$$

If $\pi \lambda \gtrsim \delta_x, \delta_y$, the force can be approximated by

$$\zeta_{\text{grd}}(z) \simeq -2\zeta_0 \frac{\pi^2 \lambda^4}{\Delta} \left(\frac{1}{\delta_x^2} e^{-(\pi \lambda / \delta_x)^2} \sin(2\pi x / \delta_x) + i \frac{1}{\delta_y^2} e^{-(\pi \lambda / \delta_y)^2} \sin(2\pi y / \delta_y) \right). \quad (27)$$

Note that the dependencies on x and y are only through the $\sin(\cdot)$ functions. Such kind of periodic functions were phenomenologically used to describe periodic or ratchet substrate-induced potentials [46,73].

The above force predicts the presence of one attractive, one repulsive, and two saddle critical points per unit cell if the driving velocity is below

$$v_{\text{th,grd}} = 2\zeta_0 \frac{\pi^2 \lambda^4}{\mathcal{N}\Delta} \min \left[\frac{e^{-(\pi \lambda / \delta_x)^2}}{\delta_x^2}, \frac{e^{-(\pi \lambda / \delta_y)^2}}{\delta_y^2} \right]. \quad (28)$$

For particular angles one could find a more restrictive threshold current. As shown in Fig. 7, the skyrmions, wherever they would be formed, will move to an attractor node. For $\zeta_0 > 0$ (attractive defects) the attractors will be close to the crossing lines, whereas for $\zeta_0 < 0$ (repulsive defects) they will be located close to the center of each cell enclosed by the defects.

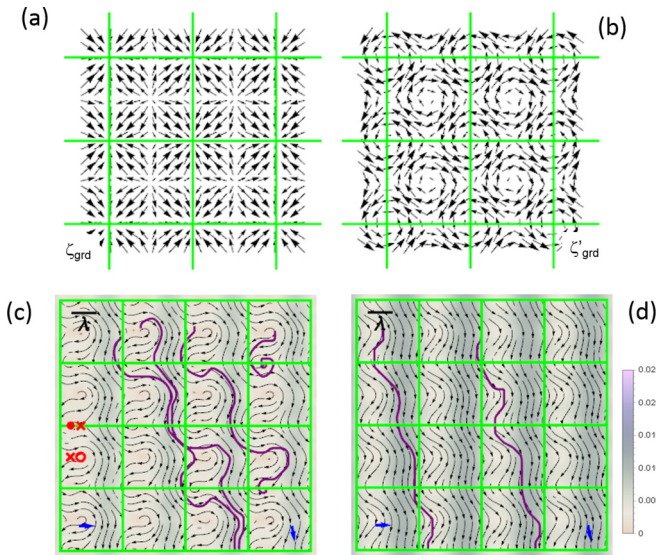


FIG. 7. Vector field (a) for ζ_{grid} and (b) for ζ'_{grid} for a grid of defects. (c),(d) Phase portraits of Thiele's equation for a grid-shaped defect. Solid purple lines correspond to the trajectories of the center of a skyrmion calculated solving the Landau-Lifshitz-Gilbert equation for several initial positions. The meanings of symbols, bars, and arrows are the same as in Fig. 3; open red circle indicates repulsive critical point [for simplicity, we have only plotted the critical point symbols in one cell in (c); they are repeated in each cell; in plot (d) there are no critical points]. For this particular example $\mathcal{G} = 3\pi$, $\mathcal{D} = 5\pi$, $\mathcal{N} = 2\pi$, $\lambda = 1$, $\zeta_0/\Delta = 0.05$, $\alpha = 0.1$, $\delta_x = \delta_y = 2.8$, and $v_h =$ (c) 0.0049 and (d) 0.0098. For the numerical calculations the local DM constant of the defect is 1.2 times the DM constant of the plain sample.

VI. FINAL REMARKS

The interaction of skyrmions with defects is a necessary ingredient in the study of their dynamics, since defects are inevitable in materials. We have modeled this interaction of skyrmions with extended defects in the shape of finite segments and different combinations of them. We have found that skyrmions can either cross line defects or be trapped by or guided along them. In the case of a gridlike defect, skyrmions can be arranged in periodic positions. Moreover, since most of our results are analytic, the points where skyrmions are trapped, the velocity of guiding along defects, or the conditions for such trapping to exist, can be obtained

as a function of the relevant parameters of the system. These parameters include the forces generated by the defects, but also the controllable agents capable of driving the skyrmions. The presented results can also be seen from another point of view: we could also engineer the skyrmion-defect interaction to better control the skyrmion dynamics. We have provided some modeling tools for developing such strategies.

We have developed expressions for the forces and threshold velocities considering extended geometries for the defects, with special attention to the case of a finite segment. We have also found that if a long defect is capable of capturing a skyrmion in one direction, the skyrmion will be guided along it with a speed independent of the strength of the defect and inversely proportional to the Gilbert constant α . When critical points appear small perturbations in the initial positions of skyrmions may result in drastically different trajectories.

Being that skyrmions are coherent emerging magnetic structures that can evolve (move) in a thin ferromagnetic layer, one can study them using generalized variables. Within the approach presented here, the internal degrees of freedom, such as deformations (including destruction or creation) or rotations are not described by the rigid model. In spite of this, direct comparison of our results with micromagnetic calculations (using the model parameters as fitting parameters) shows a good qualitative and quantitative agreement for the range of parameters used here, showing that the used potentials are a good approximation for the skyrmion-defect interaction and that the internal deformation of skyrmions is small enough to consider Thiele's equation as a useful description of the skyrmionic dynamics.

Thus, the model presented is a powerful analytic model for studying the dynamics of skyrmions in the presence of extended defects. It may help and guide further theoretical modeling of skyrmion-defects interaction considering other types of defects and also in further modeling of the interaction of skyrmions with influencing agents other than defects.

ACKNOWLEDGMENTS

We acknowledge financial support from Catalan project 2017-SGR-105 and Spanish project MAT2016-79426-P of Agencia Estatal de Investigación/Fondo Europeo de Desarrollo Regional (UE). J.C.-Q. acknowledges Grant No. FPU17/01970 from Ministerio de Ciencia, Innovación y Universidades (Spanish Government).

- [1] H. J. Queisser and E. E. Haller, *Science (New York, NY)* **281**, 945 (1998).
- [2] G. Blatter, M. V. Feigel'man, V. B. Geshkenbein, A. I. Larkin, and V. M. Vinokur, *Rev. Mod. Phys.* **66**, 1125 (1994).
- [3] L. Fang, Y. Jia, V. Mishra, C. Chaparro, V. K. Vlasko-Vlasov, A. E. Koshelev, U. Welp, G. W. Crabtree, S. Zhu, N. D. Zhigadlo *et al.*, *Nat. Commun.* **4**, 2655 (2013).
- [4] F. Banhart, J. Kotakoski, and A. V. Krasheninnikov, *ACS Nano* **5**, 26 (2011).
- [5] Z. Lin, B. R. Carvalho, E. Kahn, R. Lv, R. Rao, H. Terrones, M. A. Pimenta, and M. Terrones, *2D Mater.* **3**, 022002 (2016).
- [6] S. Yang, C. Wang, H. Sahin, H. Chen, Y. Li, S.-S. Li, A. Suslu, F. M. Peeters, Q. Liu, J. Li *et al.*, *Nano Lett.* **15**, 1660 (2015).
- [7] A. Seeger, H. Kronmüller, H. Rieger, and H. Träuble, *J. Appl. Phys.* **35**, 740 (1964).
- [8] S. Emori, U. Bauer, S.-M. Ahn, E. Martinez, and G. S. D. Beach, *Nat. Mater.* **12**, 611 (2013).
- [9] D. L. Huber, *Phys. Rev. B* **26**, 3758 (1982).
- [10] K. Y. Guslienko, B. A. Ivanov, V. Novosad, Y. Otani, H. Shima, and K. Fukamichi, *J. Appl. Phys.* **91**, 8037 (2002).
- [11] S. Mühlbauer, B. Binz, F. Jonietz, C. Pfleiderer, A. Rosch, A. Neubauer, R. Georgii, and P. Böni, *Science (New York, NY)* **323**, 915 (2009).

- [12] X. Z. Yu, Y. Onose, N. Kanazawa, J. H. Park, J. H. Han, Y. Matsui, N. Nagaosa, and Y. Tokura, *Nature (London)* **465**, 901 (2010).
- [13] N. Romming, C. Hanneken, M. Menzel, J. E. Bickel, B. Wolter, K. von Bergmann, A. Kubetzka, and R. Wiesendanger, *Science (New York, NY)* **341**, 636 (2013).
- [14] W. Jiang, P. Upadhyaya, W. Zhang, G. Yu, M. B. Jungfleisch, F. Y. Fradin, J. E. Pearson, Y. Tserkovnyak, K. L. Wang, O. Heinonen *et al.*, *Science* **349**, 283 (2015).
- [15] O. Boulle, J. Vogel, H. Yang, S. Pizzini, D. de Souza Chaves, A. Locatelli, T. O. Menteş, A. Sala, L. D. Buda-Prejbeanu, O. Klein *et al.*, *Nat. Nanotechnol.* **11**, 449 (2016).
- [16] K. Litzius, I. Lemesh, B. Krüger, P. Bassirian, L. Caretta, K. Richter, F. Büttner, K. Sato, O. A. Tretiakov, J. Förster *et al.*, *Nat. Phys.* **13**, 170 (2016).
- [17] S. Woo, K. Litzius, B. Krüger, M.-Y. Im, L. Caretta, K. Richter, M. Mann, A. Krone, R. M. Reeve, M. Weigand *et al.*, *Nat. Mater.* **15**, 501 (2016).
- [18] D. A. Gilbert, B. B. Maranville, A. L. Balk, B. J. Kirby, P. Fischer, D. T. Pierce, J. Unguris, J. A. Borchers, and K. Liu, *Nat. Commun.* **6**, 8462 (2015).
- [19] C. Moreau-Luchaire, C. Moutafis, N. Reyren, J. Sampaio, C. A. F. Vaz, N. Van Horne, K. Bouzehouane, K. Garcia, C. Deranlot, P. Warnicke *et al.*, *Nat. Nanotechnol.* **11**, 444 (2016).
- [20] A. N. Bogdanov and U. K. Röbber, *Phys. Rev. Lett.* **87**, 037203 (2001).
- [21] N. Nagaosa and Y. Tokura, *Nat. Nanotechnol.* **8**, 899 (2013).
- [22] X. Z. Yu, N. Kanazawa, Y. Onose, K. Kimoto, W. Z. Zhang, S. Ishiwata, Y. Matsui, and Y. Tokura, *Nat. Mater.* **10**, 106 (2011).
- [23] A. O. Leonov and M. Mostovoy, *Nat. Commun.* **8**, 14394 (2017).
- [24] N. Romming, A. Kubetzka, C. Hanneken, K. von Bergmann, and R. Wiesendanger, *Phys. Rev. Lett.* **114**, 177203 (2015).
- [25] W. Jiang, X. Zhang, G. Yu, W. Zhang, X. Wang, M. Benjamin Jungfleisch, J. E. Pearson, X. Cheng, O. Heinonen, K. L. Wang *et al.*, *Nat. Phys.* **13**, 162 (2016).
- [26] A. Fert, V. Cros, and J. Sampaio, *Nat. Nanotechnol.* **8**, 152 (2013).
- [27] G. Bourianoff, D. Pinna, M. Sitte, and K. Everschor-Sitte, *AIP Adv.* **8**, 055602 (2018).
- [28] R. Wiesendanger, *Nat. Rev. Mater.* **1**, 16044 (2016).
- [29] A. Fert, N. Reyren, and V. Cros, *Nat. Rev. Mater.* **2**, 17031 (2017).
- [30] X. Zhang, Y. Zhou, M. Ezawa, G. P. Zhao, and W. Zhao, *Sci. Rep.* **5**, 11369 (2015).
- [31] J. Iwasaki, M. Mochizuki, and N. Nagaosa, *Nat. Nanotechnol.* **8**, 742 (2013).
- [32] C. Reichhardt, D. Ray, and C. J. Olson Reichhardt, *Phys. Rev. Lett.* **114**, 217202 (2015).
- [33] J.-V. Kim and M.-W. Yoo, *Appl. Phys. Lett.* **110**, 132404 (2017).
- [34] W. Legrand, D. Maccariello, N. Reyren, K. Garcia, C. Moutafis, C. Moreau-Luchaire, S. Collin, K. Bouzehouane, V. Cros, and A. Fert, *Nano Lett.* **17**, 2703 (2017).
- [35] J. Iwasaki, M. Mochizuki, and N. Nagaosa, *Nat. Commun.* **4**, 1463 (2013).
- [36] K. Everschor, M. Garst, B. Binz, F. Jonietz, S. Mühlbauer, C. Pfleiderer, and A. Rosch, *Phys. Rev. B* **86**, 054432 (2012).
- [37] T. Schulz, R. Ritz, A. Bauer, M. Halder, M. Wagner, C. Franz, C. Pfleiderer, K. Everschor, M. Garst, and A. Rosch, *Nat. Phys.* **8**, 301 (2012).
- [38] J. Müller and A. Rosch, *Phys. Rev. B* **91**, 054410 (2015).
- [39] C. Hanneken, A. Kubetzka, K. von Bergmann, and R. Wiesendanger, *New J. Phys.* **18**, 055009 (2016).
- [40] J. Sampaio, V. Cros, S. Rohart, A. Thiaville, and A. Fert, *Nat. Nanotechnol.* **8**, 839 (2013).
- [41] S.-Z. Lin, C. Reichhardt, and A. Saxena, *Appl. Phys. Lett.* **102**, 222405 (2013).
- [42] Y.-H. Liu and Y.-Q. Li, *J. Phys.: Condens. Matter* **25**, 076005 (2013).
- [43] H. C. Choi, S.-Z. Lin, and J.-X. Zhu, *Phys. Rev. B* **93**, 115112 (2016).
- [44] C. Navau, N. Del-Valle, and A. Sanchez, *J. Magn. Magn. Mater.* **465**, 709 (2018).
- [45] C. Reichhardt and C. J. Olson Reichhardt, *Phys. Rev. B* **92**, 224432 (2015).
- [46] C. Reichhardt, D. Ray, and C. J. O. Reichhardt, *New J. Phys.* **17**, 073034 (2015).
- [47] J. Iwasaki, W. Koshibae, and N. Nagaosa, *Nano Lett.* **14**, 4432 (2014).
- [48] C. Navau, N. Del-Valle, and A. Sanchez, *Phys. Rev. B* **94**, 184104 (2016).
- [49] J. Müller, *New J. Phys.* **19**, 025002 (2017).
- [50] X. Zhang, J. Müller, J. Xia, M. Garst, X. Liu, and Y. Zhou, *New J. Phys.* **19**, 065001 (2017).
- [51] J. C. Martinez and M. B. A. Jalil, *New J. Phys.* **18**, 033008 (2016).
- [52] H. Yang, C. Wang, X. Wang, X. S. Wang, Y. Cao, and P. Yan, *Phys. Rev. B* **98**, 014433 (2018).
- [53] A. Thiele, *Phys. Rev. Lett.* **30**, 230 (1973).
- [54] J. Castell-Queralt, L. González-Gómez, N. Del-Valle, A. Sanchez, and C. Navau, *Nanoscale* **11**, 12589 (2019).
- [55] J. A. J. Burgess, A. E. Fraser, F. F. Sani, D. Vick, B. D. Hauer, J. P. Davis, and M. R. Freeman, *Science* **339**, 1051 (2013).
- [56] R. Badea, J. Frey, and J. Berezovsky, *J. Magn. Magn. Mater.* **381**, 463 (2015).
- [57] J. Wang, C. Jin, C. Song, H. Xia, J. Wang, and Q. Liu, *J. Magn. Magn. Mater.* **474**, 472 (2019).
- [58] L. Shen, J. Xia, G. Zhao, X. Zhang, M. Ezawa, O. A. Tretiakov, X. Liu, and Y. Zhou, *Appl. Phys. Lett.* **114**, 042402 (2019).
- [59] R. Tomasello, E. Martinez, R. Zivieri, L. Torres, M. Carpentieri, and G. Finocchio, *Sci. Rep.* **4**, 6784 (2014).
- [60] Z. Li and S. Zhang, *Phys. Rev. Lett.* **92**, 207203 (2004).
- [61] S. Zhang and Z. Li, *Phys. Rev. Lett.* **93**, 127204 (2004).
- [62] Y. B. Bazaliy, B. A. Jones, and S.-C. Zhang, *Phys. Rev. B* **57**, 3213(R) (1998).
- [63] L. Liu, O. J. Lee, T. J. Gudmundsen, D. C. Ralph, and R. A. Buhrman, *Phys. Rev. Lett.* **109**, 096602 (2012).
- [64] R. Tomasello, A. Giordano, S. Chiappini, R. Zivieri, G. Siracusano, V. Puliafito, I. Medlej, A. La Corte, B. Azzerboni, M. Carpentieri *et al.*, *Phys. Rev. B* **98**, 224418 (2018).
- [65] B. A. Ivanov, G. G. Avanesyan, A. V. Khvalkovskiy, N. E. Kulagin, C. E. Zaspel, and K. A. Zvezdin, *JETP Lett.* **91**, 178 (2010).
- [66] N. Locatelli, A. Hamadeh, F. Abreu Araujo, A. D. Belanovsky, P. N. Skirdkov, R. Lebrun, V. V. Naletov,

- K. A. Zvezdin, M. Muñoz, J. Grollier *et al.*, [Sci. Rep. **5**, 17039 \(2015\)](#).
- [67] K. Y. Guslienko and Z. V. Gareeva, [IEEE Magn. Lett. **8**, 1 \(2017\)](#).
- [68] B. Göbel, A. Mook, J. Henk, and I. Mertig, [Phys. Rev. B **99**, 020405\(R\) \(2019\)](#).
- [69] E. Haber, R. Badea, and J. Berezovsky, [J. Magn. Magn. Mater. **454**, 289 \(2018\)](#).
- [70] S. Zhang, J. Wang, Q. Zheng, Q. Zhu, X. Liu, S. Chen, C. Jin, Q. Liu, C. Jia, and D. Xue, [New J. Phys. **17**, 023061 \(2015\)](#).
- [71] I. Lima Fernandes, J. Bouaziz, S. Blügel, and S. Lounis, [Nat. Commun. **9**, 4395 \(2018\)](#).
- [72] M. Abramowitz and I. A. Stegun, *Handbook of Mathematical Functions* (Dover, New York, 1972).
- [73] C. Reichhardt, D. Ray, and C. J. Olson Reichhardt, [Phys. Rev. B **91**, 104426 \(2015\)](#).